Journal of ELECTRONIC MATERIALS, Vol. 39, No. 8, 2010
DOI: 10.1007/s11664-010-1252-y


# Electron–Electron Interactions in Sb-Doped $SnO_2$ Thin Films

TÜLAY SERIN,[1] ABDULLAH YILDIZ,[1,2,4] NECMI SERIN,[1]
NURCAN YILDIRIM,[1] FIGEN ÖZYURT,[1] and MEHMET KASAP[3]

1.—Department of Physics Engineering, Faculty of Engineering, Ankara University, 06100 Besevler, Ankara, Turkey. 2.—Department of Physics, Faculty of Science and Arts, Ahi Evran University, 40040 Kirsehir, Turkey. 3.—Department of Physics, Faculty of Science and Arts, Gazi University, Teknikokular, 06500 Ankara, Turkey. 4.—e-mail: yildizab@gmail.com

Electrical conductivity and Hall-effect measurements on undoped and Sb-doped $SnO_2$ thin films prepared by the sol–gel technique were carried out as a function of temperature (55 K to 300 K). Structural characterizations of the films were performed by atomic force microscopy (AFM) and x-ray diffraction (XRD). A doping-induced metal–insulator transition (MIT) was observed. On the metallic side of the transition, the experimental data were interpreted in terms of electron–electron interactions (EEI). The existence of EEI was confirmed by excellent agreement between theoretical and experimental data. The experimental data on the insulator side of the transition were analyzed in terms of variable-range hopping (VRH) conduction. A complete set of parameters describing the properties of the localized electrons, including hopping energy, hopping distance, and the value of the density of states at the Fermi level, was determined.

**Key words:** $SnO_2$, electrical transport, electron–electron interactions (EEI), variable-range hopping (VRH) conduction

## INTRODUCTION

Tin oxide ($SnO_2$), with a wide bandgap of 3.6 eV, is an *n*-type metallic oxide semiconductor material of great interest due to its numerous technological applications in gas sensors and solar cells.[1,2] Recently, many reports have been published on metallic oxide semiconductors such as titanium oxide ($TiO_2$) and $SnO_2$.[3–9] However, most of these studies are generally concerned with structural and optical properties. Generally, the electrical properties of $SnO_2$ are investigated by experimental direct-current (DC) conductivity data on different doped samples.

The electrical conductivity of $SnO_2$ can be changed by doping over several orders of magnitude. Control of the electrical conductivity of $SnO_2$ by adding antimony (Sb) as a donor impurity is a well-known process. At low Sb doping levels, the $[Sb^{5+}]$ state in $SnO_2$ leads to an increase in conductivity.[7] On the other hand, the Hall mobility of $SnO_2$ decreases significantly from 5 $cm^2\ V^{-1}\ s^{-1}$ to 0.1 $cm^2\ V^{-1}\ s^{-1}$ at high Sb doping levels.[7] The Hall carrier concentration is generally of the order of $10^{20}$ $cm^{-3}$ for any Sb doping level in $SnO_2$.[7] The increase in carrier concentration in $SnO_2$ is caused by replacement of a Sn atom by an added Sb atom, which gives one extra charge carrier[8] per donor impurity.

The physical properties of $SnO_2$ films also depend on the preparation technique. Although the sol–gel process has many advantages over other techniques, it is hard to correlate the optical and electrical properties of $SnO_2$ films made using this process.[9] Thus, to understand the nature of the charge transport behavior of $SnO_2$, it is necessary to perform a thorough investigation.

In order to observe the metal–insulator transition (MIT) in a material, it is generally necessary to add doping, which results in the formation of a degenerate band.[10] Conductivity changes significantly when the MIT is reached. It is possible that disordered metallic conduction can be observed due to the presence of various types of disorder in highly

(Received November 25, 2009; accepted April 18, 2010; published online May 22, 2010)

degenerate systems.[11] In such systems, electron–electron interactions (EEI) lead to a quantum correction to the classical Boltzmann conductivity on the metallic side of the MIT.[11] To the best of our knowledge, EEI effects have not been reported to date in $SnO_2$. Since EEI strongly modify the electrical transport in devices, the existence of EEI effects should be considered in the design of $SnO_2$-based devices.

In order to understand the effect of Sb doping on the electrical properties of $SnO_2$ thin films, three samples have been investigated in this work. We report measurements of the electrical transport in both undoped and Sb-doped $SnO_2$ thin films prepared by the sol–gel technique in the temperature range from 55 K to 300 K. The observed temperature behavior of the conductivity is analyzed according to the variable-range hopping (VRH) model for undoped films and using the EEI model for Sb-doped films.

## EXPERIMENTAL PROCEDURES

Rectangular-shaped 1-mm-thick (26 mm × 76 mm) glass substrates were ultrasonically cleaned in deionized water and acetone ($CH_3COCH_3$, Merck) for 30 min. They were dried in a furnace at 100°C for 10 min. $SnO_2$ and Sb:$SnO_2$ (ATO) solutions were obtained by dissolving 8.37 g stannous chloride $SnCl_22H_2O$ in 100 mL absolute ethanol ($C_2H_6O$, Merck). In order to realize Sb doping, antimony trichloride ($SbCl_3$) was dissolved in pure ethanol (20 mL). Both solutions were stirred separately and heated in closed vessels. Then the vessels were opened and the solutions stirred and heated again until the solvents completely evaporated. Finally, the dried precipitates which contained compounds of Sn and Sb were again dissolved together in 50 mL absolute ethanol. The doped solution was finally stirred and heated at 50°C for 2 h. To realize a doping concentration in the range from 0% to 4%, the Sb/Sn ratio was calculated by means of the molecular weights of $SnCI_2$ and $SbCl_3$. The cleaned glass substrates were dipped into the doped solution and withdrawn at a constant speed of 80 mm $min^{-1}$. Each coating on the glass substrate was heated at 500°C for 10 min in a furnace. This coating process was repeated to obtain the desired film thickness. Approximate film thicknesses were obtained as 500 nm from the optical transmission spectrum using the envelope method.[12]

The microstructure of the deposited films was investigated by means of an Inel-EQUINOX 1000 diffractometer. The radiation source, wavelength, and scanning range $2\theta$ of the diffractometer were Co $K_\alpha$, 0.179 nm, and 15° to 70°, respectively.

The surface morphology of the films was also observed using an SPM Solver-PRO (NT-MDT) in semicontact mode. Root-mean-square (RMS) values of surface roughness were estimated in order to study the effect of doping.

For the electrical conductivity and Hall-effect measurements by the van der Pauw method, square-shaped (5 mm × 5 mm) samples were prepared with four contacts in the corners. Using annealed indium dots, ohmic contacts to the sample were prepared, and their ohmic behavior was confirmed from current–voltage characteristics. Measurements were made at a number of temperature steps over the temperature range from 55 K to 300 K using a Lake Shore Hall-effect measurement system (HMS). At each temperature step, the Hall coefficient (with maximum 5% error) and conductivity (with maximum 0.2% error in the studied range) were measured for any possible current direction, both magnetic field directions perpendicular to the surface, and all possible contact configurations at 0.4 T (with 0.1% uniformity).

## RESULTS AND DISCUSSION

X-ray diffraction patterns of undoped and Sb-doped films are shown in Fig. 1, showing the polycrystalline structure of the samples. Matching of the observed and standard ($h$ $k$ $l$) planes confirms that the deposited films have a primitive tetragonal structure.[13] On the other hand, the preferred orientation was found to be along the (101) plane for the undoped film. However, the doped films showed a preferred orientation along the (110) plane. The lattice constants $a$ and $c$ for the tetragonal phase structure are determined by the relation

$$\frac{1}{d^2} = \left(\frac{h^2}{a^2} + \frac{k^2}{a^2}\right) + \left(\frac{l^2}{c^2}\right), \qquad (1)$$

where $d$ and ($hkl$) are the interplanar distance and Miller indices, respectively. The lattice constants $a$ and $c$ were calculated and are given in Table I. The calculated lattice constants matched well with the standard JCPDS data card.[13]

In order to determine the variation of crystallite size with doping, the size of the crystallites

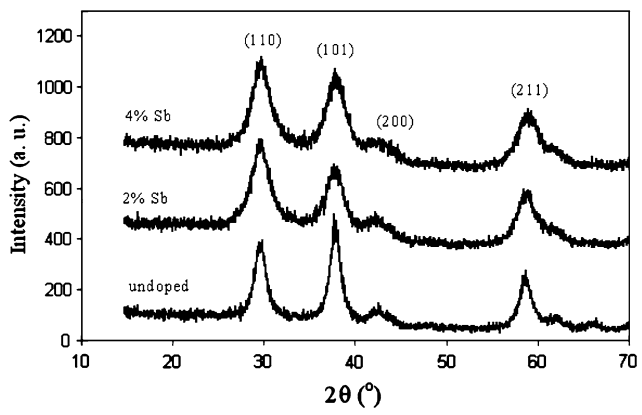


Fig. 1. XRD patterns obtained for undoped and Sb-doped $SnO_2$ films.

**Table I. Structural parameters of $SnO_2$ films**

| Samples | *a* (Å) | *c* (Å) | *c*/*a* | *L* (Å) | RMS (nm) |
|---|---|---|---|---|---|
| Undoped | 4.972 | 3.340 | 0.671 | 56.78 | 1.012 |
| 2% Sb | 4.971 | 3.363 | 0.676 | 38.30 | 1.725 |
| 4% Sb | 4.947 | 3.337 | 0.674 | 37.84 | 0.736 |

oriented along the (110) plane was calculated using Scherrer's formula[14]

$$L = \frac{0.9\lambda}{B\cos\theta}, \tag{2}$$

where $B$, $\theta$, and $\lambda$ are the broadening of the diffraction line measured at half its maximum intensity in radians, the diffraction angle, and the x-ray wavelength, respectively. The calculated values of crystallite size are given in Table I. It can be seen that the crystallite size decreases with increasing doping.

The surface morphology of the undoped and Sb-doped films is shown in Fig. 2. AFM analysis showed that the films were polycrystalline and had needle-shaped nanograins. Root-mean-square (RMS) values of surface roughness were estimated and are given in Table I. The RMS value of the 2% Sb-doped film was greater than that of the undoped film, while the RMS value of the 4% Sb-doped film was smaller than that of the undoped film.

Figure 3 shows the temperature dependence of the carrier concentration ($n$) for $SnO_2$ films in the temperature range from 55 K to 300 K. The carrier concentration of the undoped $SnO_2$ film increased as the temperature increases. However, the carrier concentrations of the Sb-doped $SnO_2$ films were nearly temperature independent. The values of carrier concentration were about $1.55 \times 10^{20}$ $cm^{-3}$ and $6.81 \times 10^{20}$ $cm^{-3}$ for the 2% Sb- and 4% Sb-doped films, respectively. Around room temperature, the Hall mobilities were 7.2 $cm^2$ $V^{-1}$ $s^{-1}$, 5.1 $cm^2$ $V^{-1}$ $s^{-1}$, and 2.2 $cm^2$ $V^{-1}$ $s^{-1}$ for the undoped, 2% Sb-, and 4% Sb-doped films, respectively. It is clear from these data that the Hall mobility of the films decreases with increasing Sb concentration, whereas the carrier concentration increases over the entire range of doping investigated. This is consistent with observations reported on $SnO_2$ films.[7,15,16]

Figure 4 shows Arrhenius plots of electrical conductivity for the $SnO_2$ films. The XRD patterns and AFM images revealed the polycrystalline structure of the samples. In polycrystalline oxides, oxygen vacancies are known to be the most common defect.[17,18] The conductivity of our undoped sample is high compared with values listed in the literature.[15,19] The high conductivity observed in the undoped film is attributed to deviation from stoichiometry due to oxygen vacancies,[20,21] which act as electron donors and increase the carrier concentration.[22] Similarly, a high carrier concentration value of $10^{19}$ $cm^{-3}$ has been reported at room temperature in undoped $SnO_2$ films.[15,16] From Fig. 4, it can be seen that the electrical conductivity of the $SnO_2$ films is increased substantially by Sb doping. $SnO_2$ is considered to be an insulator in its stoichiometric form ($SnO_2$, Sn:O = 1:2). On the other hand, in its nonstoichiometric form, $SnO_2$ can exhibit degenerate semiconductor behavior, and its conductivity becomes very high. With decreasing $O_2$ flux, the Sn concentration becomes higher in a $SnO_{2-x}$ thin film, which leads to an increase in conductivity.[23] Similar observations have been reported previously for $SnO_2$ films.[7] The conductivity of the films increased with increasing temperature. Moreover, the increase in conductivity with

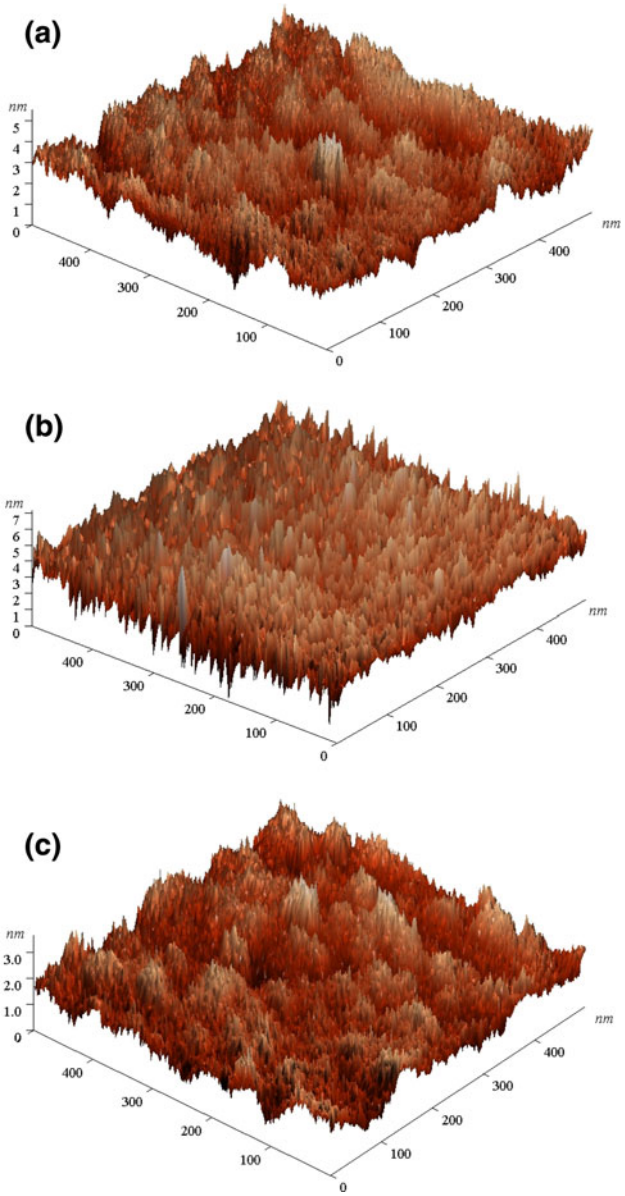


Fig. 2. Three-dimensional (3D) AFM images for (a) undoped, (b) 2% Sb-, and (c) 4% Sb-doped $SnO_2$ films.

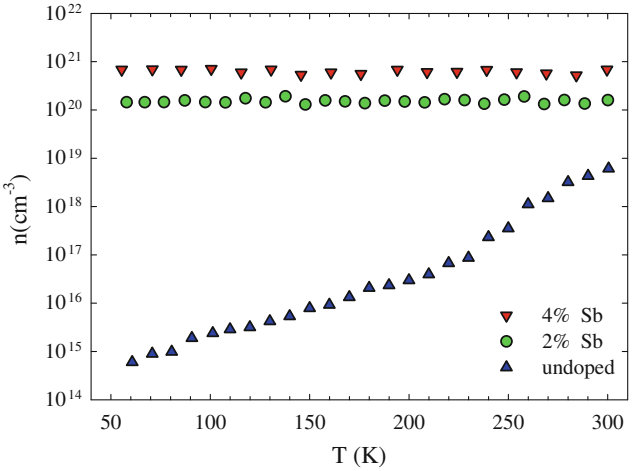


Fig. 3. Temperature dependence of the Hall carrier concentration of $SnO_2$ films in the temperature range from 55 K to 300 K.

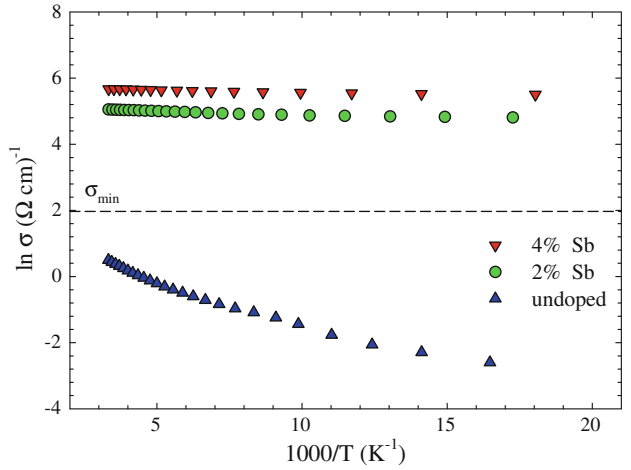


Fig. 4. Temperature dependence of the conductivity plotted as ln($\sigma$) versus 1000/$T$ in the temperature range from 55 K to 300 K.

temperature was suppressed by Sb doping. Such a situation is generally explained by the increase in Hall carrier concentration and by the formation of a degenerate band due to doping, as predicted by Mott.[11]

We failed to fit the conductivity data to the Arrhenius plot over the whole temperature range. This suggests that a simple thermal activation process does not dominate the electrical conduction in the films. Therefore, in order to better investigate the conductivity behavior of the $SnO_2$ films, a logarithmic derivation given by Zabrodskii and Zinoveva should be considered as follows[24]:

$$W(T) = \mathrm{d}[\ln \sigma(T)]/\mathrm{d}[\ln(T)]. \quad (3)$$

$W(T)$ can be used to determine the metallic and insulating behavior of the conductivity. When the slope of ln[$W(T)$] versus ln($T$) is negative, the system is on the insulating side of the MIT. A positive slope

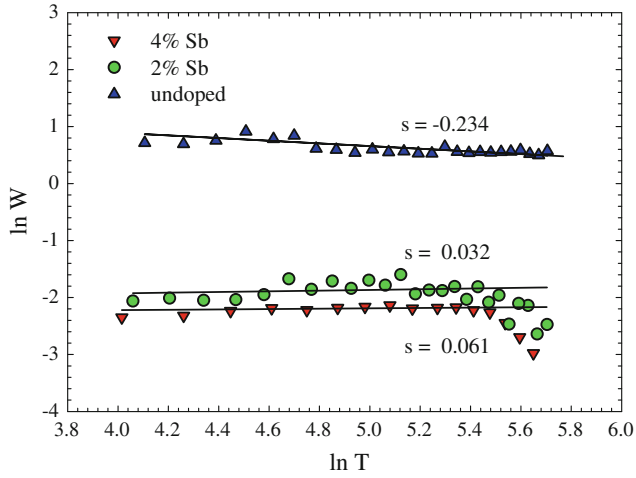


Fig. 5. Plot of ln[$W(T)$] versus ln($T$).

on the $W$ plot indicates that the system is in the metallic regime. On the other hand, the finite extrapolated value of $W(T)$ as $T \to 0$ for a material identifies the material as a weakly insulating or disordered metallic material.[24] Figure 5 shows ln[$W(T)$] versus ln($T$) for the investigated samples. The slope of $W(T)$ for the undoped sample is negative, implying that the sample is in the insulating regime, while the Sb-doped $SnO_2$ samples exhibit disordered metallic behavior with an almost temperature-independent $W(T)$. The slope of $W(T)$ gives the values $s = 0.032 \pm 0.03$ and $s = 0.062 \pm 0.01$ for 2% Sb- and 4% Sb-doped $SnO_2$, respectively. On the other hand, by making a linear regression fit to the ln[$W(T)$] versus ln($T$) plot of the undoped $SnO_2$ sample data over the whole temperature range, $s = -0.234 \pm 0.01$ is obtained (Fig. 5).

The critical carrier concentration ($n_c$) corresponding to the MIT should be known for $SnO_2$. To determine $n_c$, we have to take into consideration the Mott criterion, which is given as[10]

$$n_c^{1/3} a_B^* = 0.25, \quad (4)$$

where $a_B^*$ is the effective Bohr radius, given by the relation

$$a_B^* = 4\pi\varepsilon_0\varepsilon\hbar^2/m^* e^2, \quad (5)$$

where $\varepsilon_0$ is the permittivity of vacuum, $\hbar$ is the Planck constant, $e$ is the electron charge, $\varepsilon$ is the static dielectric constant, and $m^*$ is the effective mass. The value of $a_B^*$ is calculated as 2.54 nm by taking the values $m^* = 0.24m_0$ and $\varepsilon = 11.65$. Then we obtain $n_c = 9.54 \times 10^{17}$ cm$^{-3}$ for $SnO_2$. According to this finding, the undoped film with $n < n_c$ falls on the insulating side of the MIT for $T < 250$ K, whereas the Sb-doped films with $n > n_c$ fall on the metallic side of the MIT over the whole temperature range.

Normally, when $n$ exceeds $n_c$, the increased Coulomb interaction leads to an increase in electrical conductivity as the temperature decreases.

However, the conductivity behaviors of the Sb-doped samples show that the conductivity can be extrapolated to finite values. Hence, these two samples exhibit insulator-like behavior, although they are located above the MIT. This may arise due to the disordered structure of Sb-doped $SnO_2$. The prediction of Mott is that every disordered material must pass a minimum metallic conductivity ($\sigma_{min}$) given by[25]

$$\sigma_{min} = C\left(\frac{e^2}{a\hbar}\right), \tag{6}$$

where $a$ is the distance between centres, which is approximately equal to $n_c^{-1/3}$. $C$ is a numerical constant of the order of 0.03.[25] The value of $\sigma_{min}$ is 7.18 $\Omega^{-1}$ cm$^{-1}$ for $SnO_2$. $\sigma_{min}$ is shown in Fig. 4 by a dotted line. The Sb-doped samples with $n > n_c$ are still insulator-like, even if $\sigma > \sigma_{min}$. Such materials with high degrees of disorder can be characterized by EEI effects. So, a correction to the normal Boltzmann conductivity is required.[11] Altshular and Aronov pointed out the influence of EEI originating from static inhomogeneities in disordered systems.[26] In normal metals, the Fermi wavelength $\lambda_F$ is much smaller than the mean free path $l$ of the carriers ($\lambda_F << l$), and the Boltzmann approach can successfully describe the transport properties. However, as the structural or compositional disorder is increased, the mean free path ($l$) becomes small and eventually it may become smaller than $\lambda_F$. $\lambda_F > l$ for our Sb-doped $SnO_2$ films, as can be seen from Table II. This behavior can be explained by the presence of EEI in the system.[11,26] This leads to a quantum correction to the Boltzmann conductivity given by[26]

$$\sigma(T) = \sigma(0) + mT^{1/2}, \tag{7}$$

where $\sigma(0)$ is the zero-temperature conductivity, and the second term arises from EEI. Equation 7 was fitted to the conductivity data of Sb-doped $SnO_2$ films, and a satisfactory fit was obtained, as seen in Fig. 6. However, small deviations are seen in the higher-temperature regime for these samples. The experimental values of $m(exp.)$ are given in Table II.

A good fit to the measured data is an essential but not sufficient criterion for the applicability of the

**Table II. Values of different physical parameters of 2% Sb- and 4% Sb-doped $SnO_2$ samples**

| Parameters | 2% Sb | 4% Sb |
|---|---|---|
| $\sigma(0)$ ($\Omega^{-1}$ cm$^{-1}$) | 89.7 | 208 |
| $m(exp.)$ ($\Omega^{-1}$ cm$^{-1}$ K$^{-1/2}$) | 4.18 | 5.19 |
| $m(cal.)$ ($\Omega^{-1}$ cm$^{-1}$ K$^{-1/2}$) | 2.06 | 1.88 |
| $K$ (m$^{-1}$) | $9.08 \times 10^8$ | $1.16 \times 10^9$ |
| $F_\sigma$ | 0.202 | 0.145 |
| $l$ (Å) | 3.93 | 3.41 |
| $\lambda_F$ (Å) | 37.8 | 23.1 |
| $D$ (cm$^2$ s$^{-1}$) | 1.05 | 1.48 |

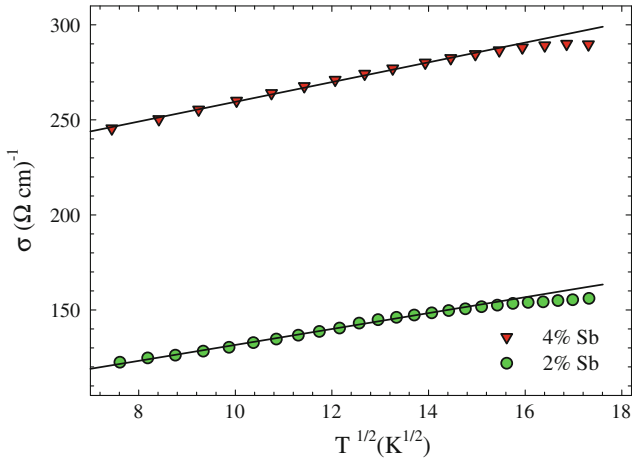


Fig. 6. Variation of conductivity as a function of $T^{1/2}$ for 2% Sb- and 4% Sb-doped $SnO_2$ films. *Solid lines* calculated by least-squares technique.

EEI model. The value of $m(cal.)$ should be calculated theoretically by the following relation[11]:

$$m = \left(\frac{e^2}{\hbar}\right)\left(\frac{1.3}{4\pi^2}\right)\left(\frac{k_B}{2\hbar D}\right)^{1/2}\left[\frac{4}{3} - (3F_\sigma/2)\right]. \tag{8}$$

In this expression, $k_B$ is the Boltzmann constant, $D$ is the diffusion coefficient, and $F_\sigma$ is an interaction parameter. $D$ is calculated with the following relation:

$$l = \frac{3\pi^2\hbar\sigma(0)}{e^2k_F^2} = \frac{3m^*D}{\hbar k_F}, \tag{9}$$

where $k_F$ is the Fermi wavevector, given by

$$k_F = \left(3\pi^2 n\right)^{1/3}. \tag{10}$$

In Eq. 8, the quantity $F_\sigma$ is related to the Fermi-liquid parameter $F$ by[26]

$$F_\sigma = \left(\frac{-32}{3}\right)\left[1 - \frac{3F}{4} - \left(1 - \frac{F}{2}\right)^{3/2}\right]F^{-1}. \tag{11}$$

The value of $F_\sigma$ is in the range between 0 and 1.[26] To calculate $F_\sigma$ the Fermi-liquid parameter $F$ is used as

$$F = \frac{1}{x}\ln(1+x), \tag{12}$$

$$x = \left(\frac{2k_F}{K}\right)^2, \tag{13}$$

where $K$ is the screening wave factor, which is given by[11]

$$K = \left(\frac{12\pi nm^*e^2}{\varepsilon\hbar^2k_F^2}\right)^{1/2}. \tag{14}$$

The calculated and fitted parameters for Sb-doped $SnO_2$ thin films are given in Table II. Reliable agreement is obtained between the experimental $m(exp.)$ and the theoretical $m(cal.)$ values, as can be seen in Table II. On the other hand, the observed difference between $m(exp.)$ and $m(cal.)$ can be explained as follows: depending on the preparation conditions, one can expect different degrees of disorder or inhomogeneity to arise in $SnO_2$. In this case, the value of carrier concentration also changes from sample to sample. We observed that $m(exp.)$ came close to $m(exp.)$ with decreasing carrier concentration. Systematic deviations become apparent when the concentration is far from the MIT, as expected.[11,26] Also, we should note that the values obtained for $m$ depend on the width of the temperature interval used. The experimental and theoretical values obtained for $m$ as well as the other parameters given in Table II are of the same order of magnitude as in a variety of disordered systems.[27–31] Here, it is interesting to note that EEI effects dominate the electron transport even at room temperature in Sb-doped films in contrast to expectations. Even if we fit Eq. 7 to the experimental conductivity data only at low temperatures, we do not obtain any considerable changes in the values of $m(exp.)$.

Returning to Fig. 4 again, one can see that the undoped $SnO_2$ is on the insulating side of the transition, since the conductivity decreases exponentially with decreasing temperature and therefore it becomes zero as $T \to 0$ K. It is also observed that $\sigma < \sigma_{min}$ for the undoped $SnO_2$. We expect that the undoped sample still exhibits insulating characteristics with its low conductivity ($\sigma < \sigma_{min}$) even if $n > n_c$ for $T > 250$ K. The temperature-dependent conductivity data give no indication of different conduction mechanisms; therefore, only VRH conduction can be considered over the whole temperature range employed in the present study. It is well known that the temperature-dependent conductivity on the insulating side of the MIT is given by the VRH model in disordered systems.[10] In the VRH model, an electron moves by hopping from one localized state to another. When the density of states is finite and the states are localized at the Fermi energy, Mott VRH occurs.[10] $\ln(\sigma)$ is proportional to $T^{-1/4}$ in Mott VRH. In this regime, three-dimensional VRH applies with a temperature-dependent $\sigma$ given by[10]

$$\sigma = \sigma_{0v} \exp\left[-\left(\frac{T_0}{T}\right)^p\right], \tag{15}$$

where $p$ is the hopping exponent, equal to 0.25 in the Mott VRH regime,[10] and

$$T_0 = \left[\frac{18\alpha^3}{k_B N(E_F)}\right], \tag{16}$$

where $T_0$ is a characteristic temperature coefficient, $\sigma_{0v}$ is a pre-exponential factor, $N(E_F)$ is the density of localized states at the Fermi level, and $\alpha$ describes the spatial extent of the localized wave function and is assumed to be 0.124 $Å^{-1}$.[10,32] Figure 7 shows a plot of $\ln(\sigma)$ against $T^{-1/4}$. The triangles in Fig. 7 represent the experimental data and the solid line the best fit. $r^2 = 0.999$ ($r$ is correlation coefficient) is obtained, which indicates a satisfactory fit. It is evident from the solid line in Fig. 7 that the electron transport of the undoped $SnO_2$ sample can be explained by the Mott VRH model. The value of $s = 0.234$ predicted from the slope of Fig. 5 also indicates that the Mott VRH conduction mechanism dominates the electrical transport in undoped $SnO_2$. In Eq. 15, $p$ (the hopping exponent) corresponds to $s$, which is shown in Fig. 5. From the slope of $\ln(\sigma)$ versus $T^{-1/4}$, $T_0$ and $N(E_F)$ can be calculated (Table III). The other hopping parameters, i.e., the temperature-dependent hopping distance ($R_{hop}$) and average hopping energy ($W_{hop}$), are given as[10]

$$R_{hop} = \left[\frac{9}{8\pi N(E_F)\alpha k_B T}\right]^{1/4}, \tag{17}$$

$$W_{hop} = \frac{3}{4\pi R_{hop}^3 N(E_F)}. \tag{18}$$

By using the value of $N(E_F)$ in Eqs. 17 and 18, the values of $R_{hop}$ and $W_{hop}$ can be obtained at 250 K. Since the product $R_{hop}\alpha = 2.47$ and $k_B T = 21.6$ meV, the requirements $R_{hop}\alpha \geq 1$ and $W_{hop} > kT$, which are essential for the validity of the Mott VRH model,

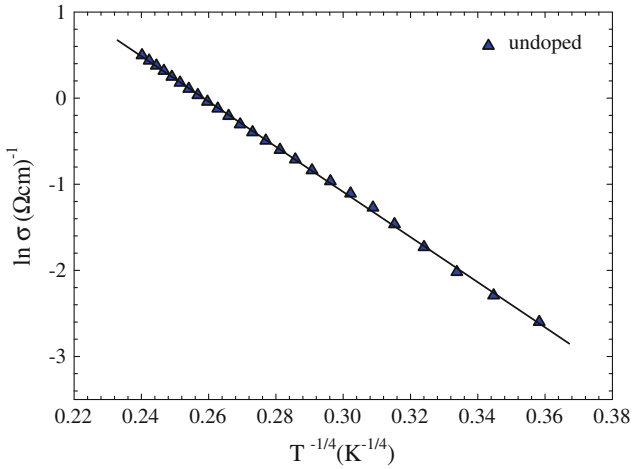


Fig. 7. Temperature dependence of the conductivity plotted as $\ln(\sigma)$ versus $T^{-1/4}$ for the undoped $SnO_2$ film in the temperature range from 55 K to 300 K. *Solid line* calculated by least-squares technique.

**Table III. Variable-range hopping parameters for undoped $SnO_2$ sample**

| $T_0$ (K) | $N(E_F)$ (cm$^{-3}$ eV$^{-1}$) | $R_{hop}$ (Å) | $W_{hop}$ (meV) |
|---|---|---|---|
| $4.74 \times 10^5$ | $8.41 \times 10^{20}$ | 19.9 | 35.6 |

are clearly satisfied. Also, the values obtained for the VRH parameters are of the same order of magnitude as those found in a variety of disordered systems.[3,33–36] This indicates that conduction in the temperature range investigated is due to VRH in the undoped film.

## CONCLUSIONS

Electrical conductivity, Hall-effect, XRD, and AFM measurements were carried out on undoped and Sb-doped $SnO_2$ thin films prepared by the sol–gel technique. The temperature-dependent Hall-effect and conductivity measurements show a doping-induced MIT. It was observed that the Sb-doped $SnO_2$ thin films were on the metallic side of the MIT, whereas the undoped $SnO_2$ thin film was on the insulating side of the MIT. Electrical conduction in Sb-doped $SnO_2$ thin films can be well expressed by a model that takes into account EEI, while the behavior of the undoped $SnO_2$ thin film is explained by a VRH model between localized states. Various electrical parameters of the films were found to be appropriate for the EEI and VRH regimes.

## ACKNOWLEDGEMENTS

This work is supported by the State of Planning Organization of Turkey under Grant No. 2001K120590 and the Ankara University BAP under Project Number 2007-07-45-054. We would also like to thank Prof. Dr. Yusuf Kağan Kadıoğlu and Ms. Murat Yavuz for providing XRD and AFM measurements.

## REFERENCES

1. G. Zhang and M. Liu, *Sens. Actuators B: Chem.* 69, 144 (2000).
2. N. Barsan and U. Weimar, *J. Phys.: Condens. Matter* 15, R813 (2003).
3. A. Yildiz, S.B. Lisesivdin, M. Kasap, and D. Mardare, *J. Non-Cryst. Solids* 354, 4944 (2008).
4. A. Yildiz, S.B. Lisesivdin, M. Kasap, and D. Mardare, *Physica B* 404, 1423 (2009).
5. T. Serin, N. Serin, S. Karadeniz, H. Sarı, N. Tuğluoğlu, and O. Pakma, *J. Non-Cryst. Solids* 352, 209 (2006).
6. A.J.C. Lanfredi, R.R. Geraldes, O.M. Berengue, E.R. Leite, and A.J. Chiquito, *J. Appl. Phys.* 105, 023708 (2009).
7. C. Terrier, J.P. Chatelon, and J.A. Roger, *Thin Solid Films* 295, 95 (1997).
8. W.A. Badawy and E.A. El-Taher, *Thin Solid Films* 158, 277 (1988).
9. V. Geraldo, L.V.A. Scalvi, E.A. Morais, C.V. Santilli, and S.H. Pulcinelli, *Mater. Res.* 6, 451 (2003).
10. N.F. Mott and E.A. Davis, *Electronic Processes in Non-Crystalline Materials* (Oxford: Clarendon, 1971).
11. P.A. Lee and T.V. Ramakrishnan, *Rev. Mod. Phys.* 57, 287 (1985).
12. R. Swanepoel, *J. Phys. E Sci. Instrum.* 16, 1214 (1983).
13. JCPDS Card no 41-1445 (Tetragonal $SnO_2$).
14. B.D. Cullity, *Elements of X-Ray Diffraction*, 2nd ed. (Reading, MA: Addison-Wesley, 1978).
15. E. Elangovan, K. Ramesh, and K. Ramamurthi, *Solid State Commun.* 130, 523 (2004).
16. E. Elangovana, S.A. Shivashankar, and K. Ramamurthia, *J. Cryst. Growth* 276, 215 (2005).
17. J. Jin, C. Seong-Pyung, C.C. Ik, S.D. Chan, P.J. Sung, B.-T. Lee, and P. Yeong-Jun, *Solid State Commun.* 127, 595 (2003).
18. J. Ma, Y. Wang, F. Ji, X. Yu, and H. Ma, *Mater. Lett.* 59, 2142 (2005).
19. E.Kh. Shokr, M.M. Wakkad, H.A. Abd El-Ghanny, and H.M. Ali, *J. Phys. Chem. Solids* 61, 75 (2000).
20. A.F. Carroll and L.H. Slack, *J. Electrochem. Soc.* 123, 1889 (1976).
21. I.S. Mulla, A.S. Soni, V.J. Rao, and A.P. Sinha, *J. Mater. Sci.* 21, 1280 (1986).
22. J.C. Fan and B. Goodenough, *J. Appl. Phys.* 48, 3524 (1977).
23. P.Y. Liua, J.F. Chenb, and W.D. Sun, *Vacuum* 76, 7 (2004).
24. A.G. Zabrodskii and K.N. Zinoveva, *Phys. JETP* 59, 425 (1984).
25. M. Kaveh and N.F. Mott, *J. Phys. C: Solid State Phys.* 15, L697 (1982).
26. B.L. Altshuler and A.G. Aronov, *Electron-Electron Interactions in Disordered Systems*, ed. A.L. Efros and M. Pollak (New York: North-Holland, 1985), .
27. K. Lal, A.K. Meikap, S.K. Chattopadhyay, S.K. Chatterjee, M. Ghosh, A. Barman, and S. Chatterjee, *Solid State Commun.* 113, 533 (2000).
28. P.N. Vishwakarma and S.V. Subramanyam, *Philos. Mag.* 87, 811 (2007).
29. D. Biswas, A.K. Meikap, S.K. Chattopadhyay, and S.K. Chatterjee, *Physica B* 382, 51 (2006).
30. A. Yildiz, S.B. Lisesivdin, M. Kasap, and M. Bosi, *Solid State Commun.* 149, 337 (2009).
31. A. Yildiz, S.B. Lisesivdin, P. Tasli, E. Ozbay, and M. Kasap, *Curr. Appl. Phys.* 10, 838 (2010).
32. H. Fritsche, *Amorphous and Liquid Semiconductors*, ed. J. Tauc (London: Plenum, 1974), .
33. K. Dutta and S.K. De, *Mater. Lett.* 61, 4967 (2007).
34. A. Yildiz, N. Serin, T. Serin, and M. Kasap, *Jpn. J. Appl. Phys.* 48, 111203 (2009).
35. A. Yildiz, S.B. Lisesivdin, H. Altuntas, M. Kasap, and S. Ozcelik, *Physica B* 404, 4202 (2009).
36. A. Yildiz, S.B. Lisesivdin, M. Kasap, and D. Mardare, *J. Mater. Sci: Mater. Electron.* doi:10.1007/s10854-009-9979-z.